Int J Interact Des Manuf (2013) 7:37–49
DOI 10.1007/s12008-012-0163-y

ORIGINAL PAPER

A simple and robust method for spiral bevel gear generation and tooth contact analysis

Julien Astoul · Jérôme Geneix · Emmanuel Mermoz · Marc Sartor

Received: 16 June 2011 / Accepted: 6 April 2012 / Published online: 24 April 2012

Abstract A simple and robust method to simulate spiral bevel gears generating and meshing processes is proposed. In a first part, a mathematical model of universal hypoid tooth surfaces generator is formulated. It is based on Fong's approach. The model takes into account all the kinematic motions of common CNC machine tools dedicated to hypoid gears machining. It is general enough to enable the simulation of various hypoid gears cutting methods such as face-hobbing, face-milling, plunge cutting and bevel-worm-shaped-hobbing processes. In this paper, only developments related to face-milled spiral bevel gear generation are presented. We show that the results obtained are in good agreement with those of certified software. In a second part, a simple and numerically stable algorithm is proposed for unloaded tooth contact analysis. The simulation method is based on a discretization of one of the two tooth flank surfaces in contact and a specific projection of the points on the opposite flank. It gives a good approximation of the contact pattern location. The accuracy of the contact point locations and computing time is directly dependent on the mesh density. However, this approach enables obtaining in a very short time sufficiently accurate results to meet the needs of designers, particularly in the preliminary stages of design. The relative displacements of the gears can be taken into consideration. The robustness of the proposed computing process and the adjustable accuracy of the results are the two main advantages of the presented approaches.

Keywords Spiral bevel gear · Hypoid gear · Tooth surface generation · Tooth contact analysis · Mathematical model

J. Astoul (✉) · J. Geneix · E. Mermoz
Eurocopter, Aéroport International Marseille Provence,
13725 Marignane Cedex, France
e-mail: julien.lab1@gmail.com
e-mail: julien.astoul@eurocopter.com

M. Sartor
Université de Toulouse, INSA, ISAE, EMAC, UPS, Institut Clément Ader (ICA), 135 avenue de Rangueil, 31077 Toulouse, France
e-mail: marc.sartor@insa-toulouse.fr

Abbreviations

A	Machine center to cross point
A_m, A_s	Axial displacement of the master part, of the slave part
B	Sliding base
E	Work offset
G_w	Outer cone distance of the tooth
i	Tilt angle
j	Swivel angle
L_{pt}	3×3 upper-left submatrix of M_{wt} system
$\vec{n}_t$	Unit normal vector to tool surface
$\vec{n}_p$	Unit normal vector to workpiece surface
O	Offset displacement
p_m, p_s	Angular pitch of the master part, of the Slave part
R_f	Filet radius of the tool
R_p	Profile radius of the tool
R_t	Mean radius of the tool
R_w, R_s	Sphere radius of the workpiece
$\vec{r}_t$	Position vector in tool system
$\vec{r}_p$, $\vec{r}_m$, $\vec{r}_s$	Position vector in workpiece system
$\vec{r}_{\theta s}$	Master point position vector in slave part system
S	Radial distance
s_t	Curvilinear abscissa along the tool section
XW_f	Point radius of the tool
W_f	Point width of the tool

W_w	Face width of the tooth
α_p	Profile angle of the tool
γ	Shaft angle between the master and the Slave part
γ_f	Root cone angle of the tooth profile
γ_h	Head cone angle of the tooth profile
γ_w, γ_s	Cone angle of the workpiece
Γ	Machine root angle
δc	Distance between master part point and Slave part flank
θ_m	Rotation angle of the master part in the Meshing process
ϕ_c	Rotation angle of the cradle in the generation process
ϕ_t	Rotation angle of the tool in the generation process
ϕ_p, ϕ_s	Rotation angle of the workpiece in the generation process
φ	Tool rotation angle in the face-hobbing process

1 Introduction

The spiral bevel gears are components of many high-tech devices. Because of a relatively complex geometry, continuous efforts are made to streamline the design and manufacturing process. The performance improvements rely on the means to analyze and control all the phenomena appearing in these mechanisms. The implementation of numerical tools to build, from the earliest stages of design, an accurate representation of surfaces that will be then machined is still an open field of study. There are many ways to approach the subject. The choices can have significant consequences in terms of precision, reliability and cost. The ability to develop a simple, robust, and universal method remains an important issue. This is also true for the tooth contact analysis of the spiral bevel gears.

The literature provides numerous papers dealing with spiral bevel and hypoid gear generation. Most methods are based on the theory of surface envelopes. "Theory of gearing" by Litvin [17] details this approach. It involves complex geometry and relative motions. The solving method relies on the use of reference systems. Di Puccio [1,2] shows that the theory of gearing can be formulated without any recourse to reference systems. This invariant approach is entirely based on geometric concepts. As an example, Di Puccio [3] and Gabiccini [9] apply this new method to the generation of spiral bevel and hypoid gears. Dooner [4,5] uses another approach of the theory of gearing: the theory of screws. There are various manufacturing processes for the spiral bevel and hypoid gears. The two mains are face-milling and face-hobbing. Litvin [12] is one of the first to develop a computer simulation of the spiral bevel gear machining process. He considers the Gleason technology. Each tooth results from the tool work envelope. Later, Litvin [13] proposes a numerical model of the Gleason Phoenix CNC machine tool. Lin [10] presents a model made of four components. The first part is the tool geometry. The second defines the modified roll method. The third is the kinematic relation between the tool and the workpiece. The fourth introduces the equation of meshing which rules the generation process. Fong [8] proposes a mathematical model to make easier the development of a universal hypoid gear generator. Despite its simplicity, it enables to virtually simulate most of the existing processes. More recently, Shih [19] adapts Fong's model to simulate other face-hobbing processes.

The earliest study of Litvin [11] about the behavior of the spiral bevel gear focuses on theoretical models approximating the practically non conjugate tooth surfaces by theoretically conjugated ones. However, these hypothetical conjugate surfaces are simpler than the actual ones and the meshing motion is extremely sensitive to the flank shapes. The simulation of the spiral bevel gear machining process is the only way to obtain exact tooth topographies and a good estimation of the contact pattern location. Therefore, Litvin et al. [14–16] develop a tooth contact analysis method directly related to the physical machine tool kinematic motions. Vogel [21] proposes a direct mathematical model relying on the same approach. The research and generation of the contact points run simultaneously. However, it requires the numerical resolution of many non linear equations. The instability risk is high and it does not simplify the convergence management. Fan [6,7] generalizes his model to face-milling and face-hobbing processes. He proposes to reduce the number of nonlinear equations to be considered and thus improves the stability of the meshing simulation algorithm. The core of his approach is the determination of the contact point location at each phase of engagement by solving a system of five nonlinear equations. Three of them imply the punctual coincidence of the pinion and gear tooth surfaces. The two others involve the tangency between the mating tooth flanks. They formalize the contact point existence conditions. Sheveleva [18] proposes an algorithm based on the examination of the distance field between the two mating tooth surfaces. This approach avoids having to solve a heavy system of nonlinear equations. Vimercati [20] applies finite element method with a low torque. The results are similar for a longer computing time.

A method based on the simplest approaches is defined in this paper. The proposed algorithm is very stable and gives quickly a good approximation of the contact pattern location. The balance between accuracy and computing time is adjustable. The level of complexity is reduced to achieve a high robustness. The simulation algorithm has to run whatever the tooth flank topography without being at fault. The goal is, in fine, to achieve an automated improvement process of

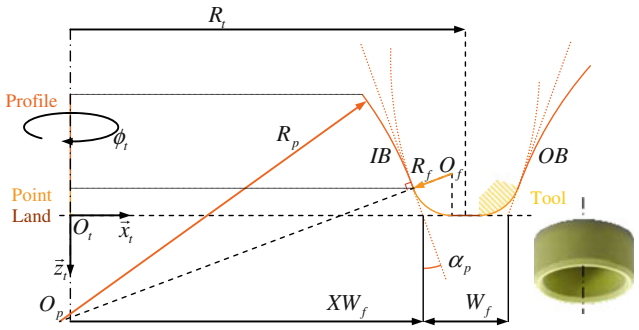

Fig. 1 Tool transverse section geometry

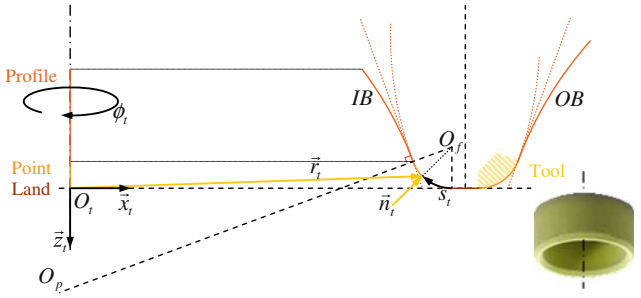

Fig. 2 Tool surface parameterization

the behavior of the spiral bevel gear relying on a direct optimization of the machine tool settings.

In a first time, the mathematical method used to model the nominal surfaces of spiral bevel gear flanks that will be machined is detailed. It is based on Fong's approach [8]. It enables reducing the number of equations which have to be solved numerically. In this paper, the simplifications are clearly highlighted. They make easier the development process and the algorithm convergence management. In a second time, a meshing simulation algorithm is presented. The general approach is similar to that of Sheveleva [18] but the calculation method used differs. In this paper, the distance measurement is performed from generated points when Sheveleva uses interpolations. The accuracy of distance measurement values is thus higher. The simplicity and the robustness of the proposed approach are illustrated. Finally, we conclude with the interest of such qualities for the future works.

2 Spiral bevel gear generation

2.1 Mathematical model

2.1.1 Tool settings

The tool considered here as the basis of the tooth flank generation is made of surfaces of revolution. Its transverse section is shown in Fig. 1 The inside and outside tool flanks (IB and OB in Fig. 1) generate respectively the convex and concave tooth flanks. A tool flank is made of three parts. The profile is either a conical or a toroidal surface. It machines the tooth flank profile. As shown in Fig. 1, it can be concave, straight or convex. The point is a convex toroidal surface. It produces the tooth flank root. The land is a plane surface. It makes the tooth root land. The contiguous parts intersect satisfying positional and tangential continuity.

The tool surface is defined using two parameters. The curvilinear abscissa along the transverse section and the rotation angle of the tool are drawn in Fig. 2

The position vector of a point on the flank surface is defined in the tool Cartesian system as shown in Eq. (1).

$$\vec{r}_t = \begin{bmatrix} x_t\,(s_t, \phi_t) \\ y_t\,(s_t, \phi_t) \\ z_t\,(s_t, \phi_t) \\ 1 \end{bmatrix} \tag{1}$$

Then, the unit normal vector to flank surface at this point is determined as shown in Eq. (2).

$$\vec{n}_t = \frac{\frac{\partial \vec{r}_t}{\partial s_t} \times \frac{\partial \vec{r}_t}{\partial \phi_t}}{\left\| \frac{\partial \vec{r}_t}{\partial s_t} \times \frac{\partial \vec{r}_t}{\partial \phi_t} \right\|} = \begin{bmatrix} u_t\,(s_t, \phi_t) \\ v_t\,(s_t, \phi_t) \\ w_t\,(s_t, \phi_t) \end{bmatrix} \tag{2}$$

2.1.2 Machine tool settings

The mathematical model is potentially able to simulate six axes CNC machine tool. It takes into account fourteen settings: the machine center to cross point, the machine root angle, the sliding base, the work offset, the radial distance, the swivel angle, the tilt angle, the tool rotation angle and the six modified roll coefficients of the cradle rotation angle. The modified roll method consists of a representation of the machine settings in higher order polynomials in terms of the workpiece increment angle. It enables accurate modifications of the tooth flank topographies. Figures 3 and 4 describe the machine tool kinematic model.

The machine tool kinematic motions shown in Fig. 4 are not really used to generate face-milled spiral bevel gears. The swivel angle, the tilt angle and the tool rotation angle are set to zero. Nevertheless, all of them are implemented in the tooth flank generation algorithm.

The present work is illustrated with an example of spiral bevel gear manufactured with the face-milling method. The machine tool architecture enables recreating the meshing motion between the workpiece and an imaginary generating gear as shown in Fig. 5. The tool materializes a gear tooth and thus follows the same trajectory. It turns around the cradle axis which is that of the gear. So, the cradle motion depends on the workpiece rotation.

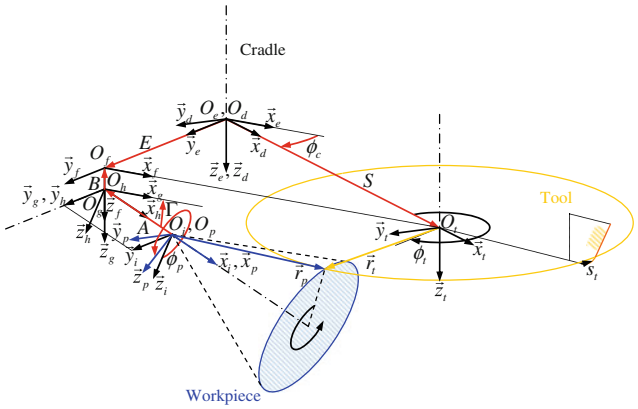

Fig. 3 General machine tool kinematic motions

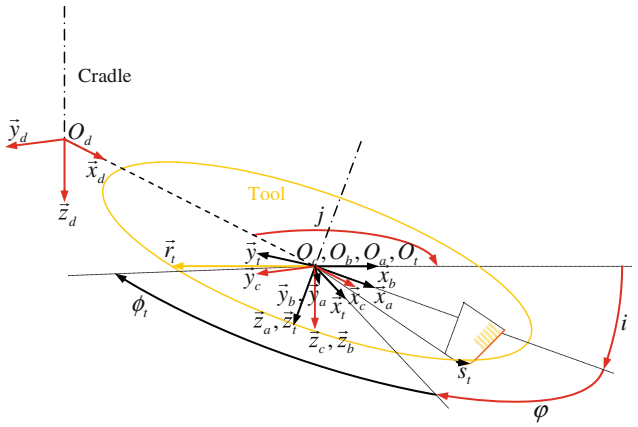

Fig. 4 Optional machine tool kinematic motions

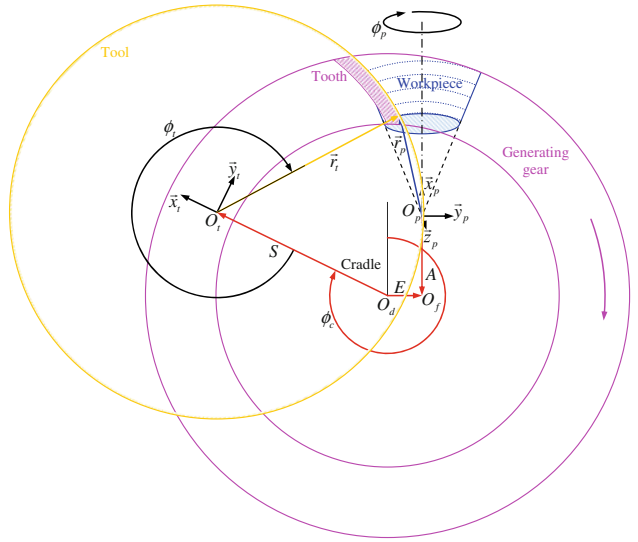

Fig. 5 Simulation of the generating gear meshing with the workpiece

The generation of face-milled spiral bevel gears requires a relation linking the cradle to the workpiece rotation angle. A roll ratio is applied between the cradle and workpiece angles. Its function is changed and extended with the modified roll method. The tooth flank topographies are thus changed. The Eq. (3) gives the representation of the cradle angle in terms of the workpiece angle. The first coefficient of the polynomial is the roll ratio. The whole polynomial is usually known as the modified roll ratio. Figure 6 shows the specific effect of each coefficient on the tooth flank surfaces.

$$\phi_c\left(\phi_p\right) = \phi_{c0} + c_1 \cdot \phi_p + \frac{c_2}{2!} \cdot \phi_p^2 + \frac{c_3}{3!} \cdot \phi_p^3 + \frac{c_4}{4!} \cdot \phi_p^4 + \frac{c_5}{5!} \cdot \phi_p^5 + \frac{c_6}{6!} \cdot \phi_p^6 \tag{3}$$

2.1.3 Generation method

The tool generates the blank between two teeth of the workpiece as shown in Fig. 7. Its motion generates a family of surfaces. The tooth flank surface is the resulting envelope. The generation method is based on the differential geometry.

Theoretically, the envelope exists at the point where the tool surface normal is perpendicular to its velocity defined relatively to the envelope system. That is mathematically formalized by the equation of meshing shown in Eq. (4). A generated point of the workpiece tooth flank exists if this equation is satisfied.

$$f_p = \vec{n}_p \cdot \frac{\partial \vec{r}_p}{\partial \phi_p} = 0 \tag{4}$$

The position of a point on the tool flank surface is defined in the workpiece Cartesian system as shown in Eq. (5).

$$\vec{r}_p = M_{pt} \cdot \vec{r}_t = \begin{bmatrix} x_p & \left(s_t, \phi_t, \phi_p\right) \\ y_p & \left(s_t, \phi_t, \phi_p\right) \\ z_p & \left(s_t, \phi_t, \phi_p\right) \\ & 1 \end{bmatrix} \tag{5}$$

The tool flank surface normal at this point is defined in the workpiece Cartesian system as shown in Eq. (6).

$$\vec{n}_p = L_{pt} \cdot \vec{n}_t = \begin{bmatrix} u_p & \left(s_t, \phi_t, \phi_p\right) \\ v_p & \left(s_t, \phi_t, \phi_p\right) \\ w_p & \left(s_t, \phi_t, \phi_p\right) \end{bmatrix} \tag{6}$$

The coordinate transformation matrix from the tool system to the workpiece system is shown in Eq. (7). The different elementary transformation matrices formalize the machine tool architecture illustrated in Figs. 3 and 4.

$$M_{pt} = M_{pi} \cdot M_{ih} \cdot M_{hg} \cdot M_{gf} \cdot M_{fe} \cdot M_{ed} \cdot M_{dc} \cdot M_{cb} \cdot M_{ba} \cdot M_{at} \tag{7}$$

$$M_{pi} = \begin{bmatrix} 1 & 0 & 0 & 0 \\ 0 & \cos\left(\phi_p\right) & -\sin\left(\phi_p\right) & 0 \\ 0 & \sin\left(\phi_p\right) & \cos\left(\phi_p\right) & 0 \\ 0 & 0 & 0 & 1 \end{bmatrix} \quad M_{ih} = \begin{bmatrix} 1 & 0 & 0 & -A \\ 0 & 1 & 0 & 0 \\ 0 & 0 & 1 & 0 \\ 0 & 0 & 0 & 1 \end{bmatrix}$$

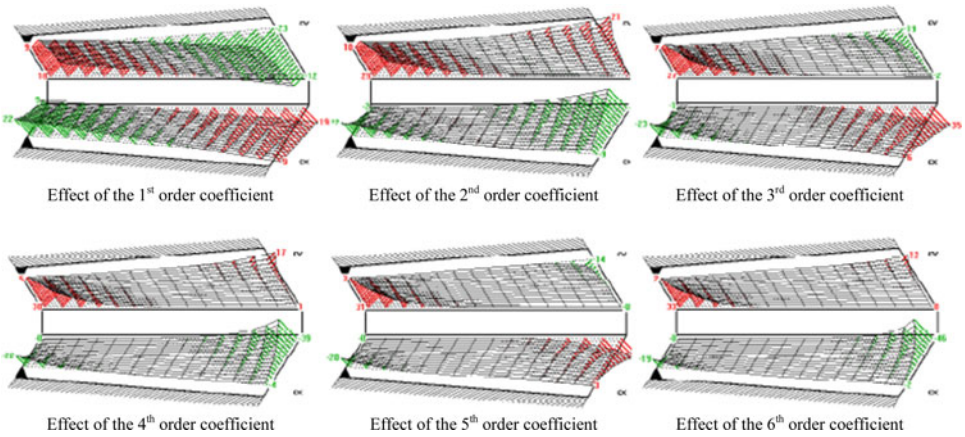

Fig. 6 Effects of the modified roll coefficients on the tooth flank topographiesFigure caption

$$M_{hg} = \begin{bmatrix} \cos(\Gamma) & 0 & \sin(\Gamma) & 0 \\ 0 & 1 & 0 & 0 \\ -\sin(\Gamma) & 0 & \cos(\Gamma) & 0 \\ 0 & 0 & 0 & 1 \end{bmatrix} \quad M_{gf} = \begin{bmatrix} 1 & 0 & 0 & 0 \\ 0 & 1 & 0 & 0 \\ 0 & 0 & 1 & -B \\ 0 & 0 & 0 & 1 \end{bmatrix}$$

$$M_{fe} = \begin{bmatrix} 1 & 0 & 0 & 0 \\ 0 & 1 & 0 & E \\ 0 & 0 & 1 & 0 \\ 0 & 0 & 0 & 1 \end{bmatrix} \quad M_{ed} = \begin{bmatrix} \cos(\phi_c) & \sin(\phi_c) & 0 & 0 \\ -\sin(\phi_c) & \cos(\phi_c) & 0 & 0 \\ 0 & 0 & 1 & 0 \\ 0 & 0 & 0 & 1 \end{bmatrix}$$

$$M_{dc} = \begin{bmatrix} 1 & 0 & 0 & S \\ 0 & 1 & 0 & 0 \\ 0 & 0 & 1 & 0 \\ 0 & 0 & 0 & 1 \end{bmatrix} \quad M_{cb} = \begin{bmatrix} -\sin(j) & -\cos(j) & 0 & 0 \\ \cos(j) & -\sin(j) & 0 & 0 \\ 0 & 0 & 1 & 0 \\ 0 & 0 & 0 & 1 \end{bmatrix}$$

$$M_{ba} = \begin{bmatrix} \cos(i) & 0 & \sin(i) & 0 \\ 0 & 1 & 0 & 0 \\ -\sin(i) & 0 & \cos(i) & 0 \\ 0 & 0 & 0 & 1 \end{bmatrix}$$

$$M_{at} = \begin{bmatrix} \cos(\varphi) & -\sin(\varphi) & 0 & 0 \\ \sin(\varphi) & \cos(\varphi) & 0 & 0 \\ 0 & 0 & 1 & 0 \\ 0 & 0 & 0 & 1 \end{bmatrix}$$

Three variables run the generation process: the curvilinear abscissa along the tool section, the rotation angle of the tool and the rotation angle of the workpiece. Usually, we assume the workpiece rotation angle is a polynomial function of the cradle rotation angle. This relation may be considered as bijective. Hence, we can also define the cradle rotation angle as a polynomial function of the workpiece rotation angle as shown in Eq. (3). This trick simplifies the manipulation of the equation of meshing. This equation is extended, simplified and factorized to establish the Fong formulation [8].

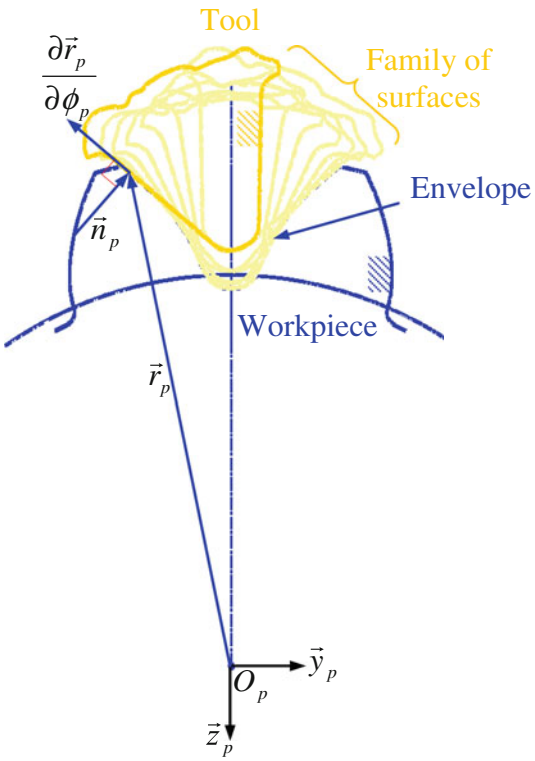

Fig. 7 Generation of the envelope

Its analytical solution gives the rotation angle of the tool as a function of the curvilinear abscissa along the tool section and the workpiece rotation angle.

2.1.4 Generation of the tooth root

The tooth flank points are generated on spheres which are centered on the pitch apex as shown in Fig. 8. The pitch apex is the workpiece pitch cone center. The tool point machines the tooth flank root. The curvilinear abscissas of the points

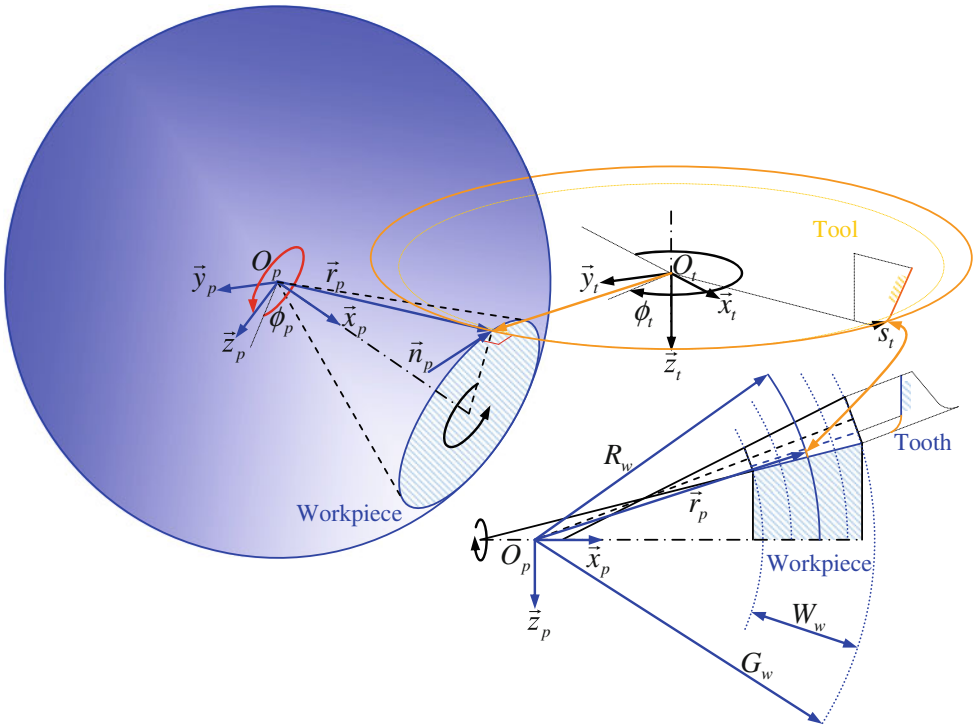

Fig. 8 Generation of the tooth root

along the tool point and the sphere radiuses are known. The tool and workpiece rotation angles are unknown. The problem is solved with the two independent equations written in Eqs. (8) and (9).

The equation of meshing gives the tool rotation angle in terms of the workpiece rotation angle as shown in Eq. (8).

$$f_p(\phi_t, \phi_p) = 0 \Rightarrow \phi_t = f(\phi_p) \tag{8}$$

The existence condition of the tooth root points on the given spheres is formalized by Eq. (9).

$$\sqrt{x_p^2(\phi_p) + y_p^2(\phi_p) + z_p^2(\phi_p)} - R_w = 0 \tag{9}$$

Equation (8) is solved analytically and Eq. (9) is solved numerically with the Newton–Raphson method. Equations (8) and (9) are solved simultaneously and the coordinates of the generated points are determined.

2.1.5 Generation of the tooth profile

The points of the tooth profile are generated at the intersections of spheres and cones as shown in Fig. 9. The spheres and cones are centered on the pitch apex. The sphere radiuses and the cone angles are known. The tool and workpiece rotation angles are unknown. The curvilinear abscissas of the points along the tool profile are not given. The two following Equations (10) and (11) are not sufficient to solve the problem. Hence, one more equation is formulated in Eq. (12).

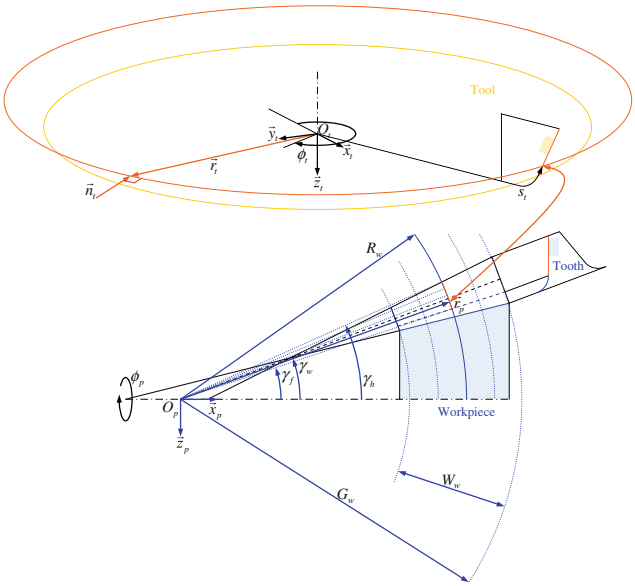

Fig. 9 Generation of the tooth profile

The equation of meshing gives the tool rotation angle in terms of the curvilinear abscissa of the point along the tool profile and the workpiece rotation angle as shown in Eq. (10).

$$f_p(s_t, \phi_t, \phi_p) = 0 \Rightarrow \phi_t = f(s_t, \phi_p) \tag{10}$$

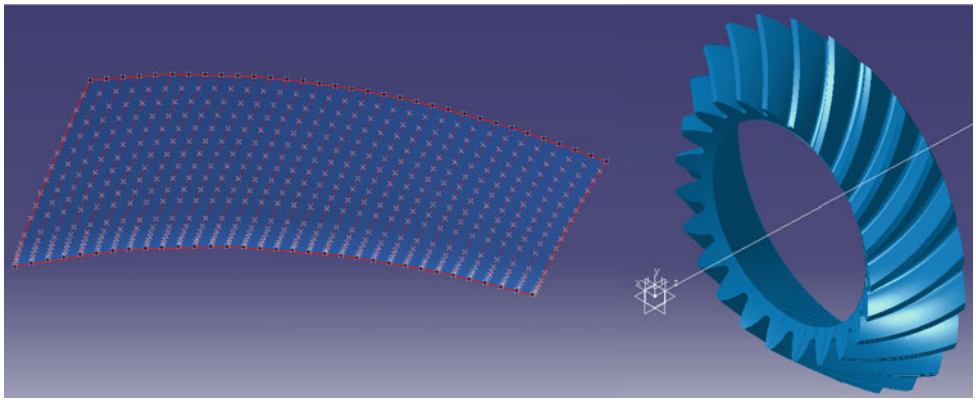

Fig. 10 Points used to build the CAO model

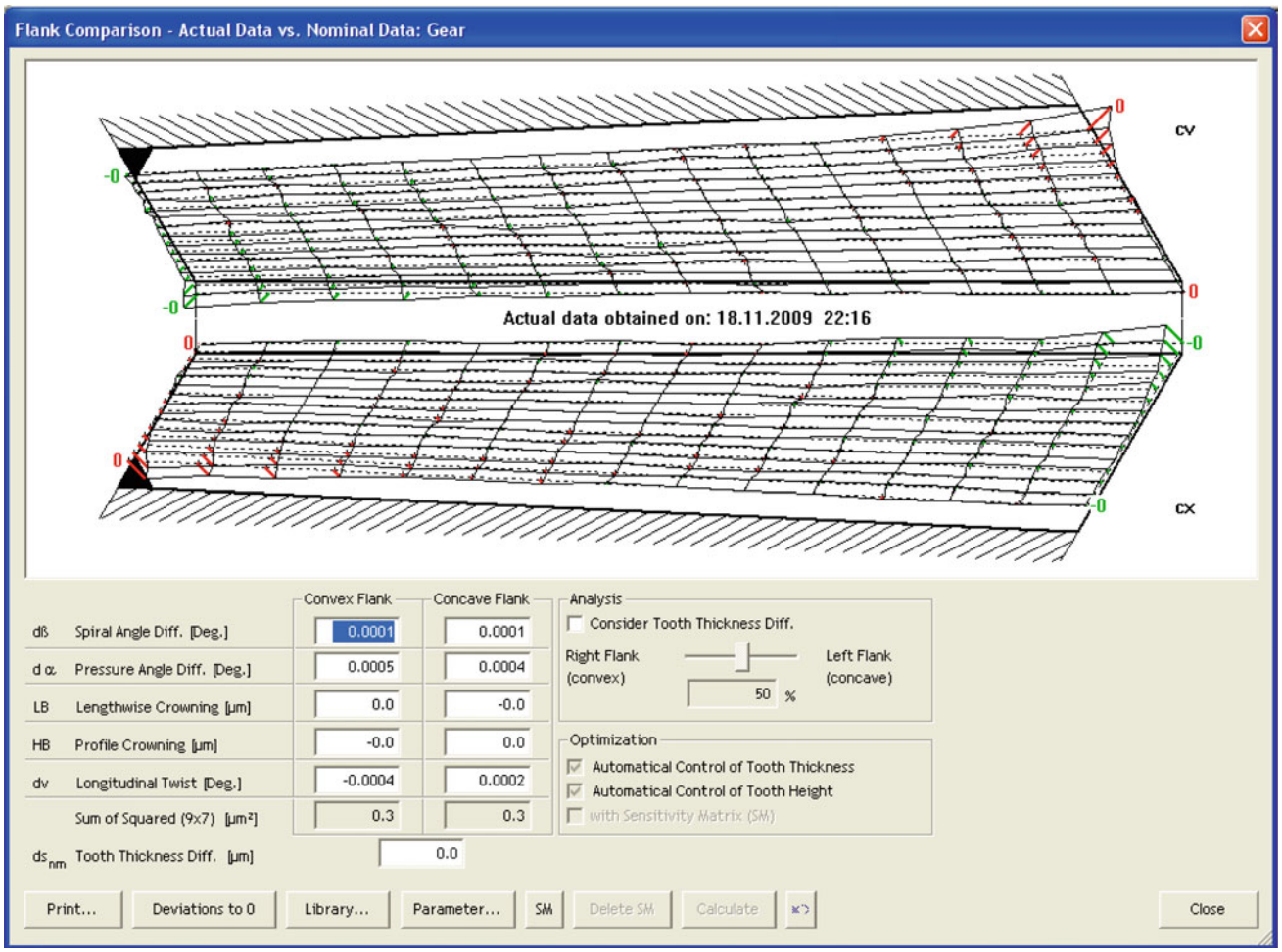

Fig. 11 Comparison with existing generation software

Fig. 12 Relative displacements

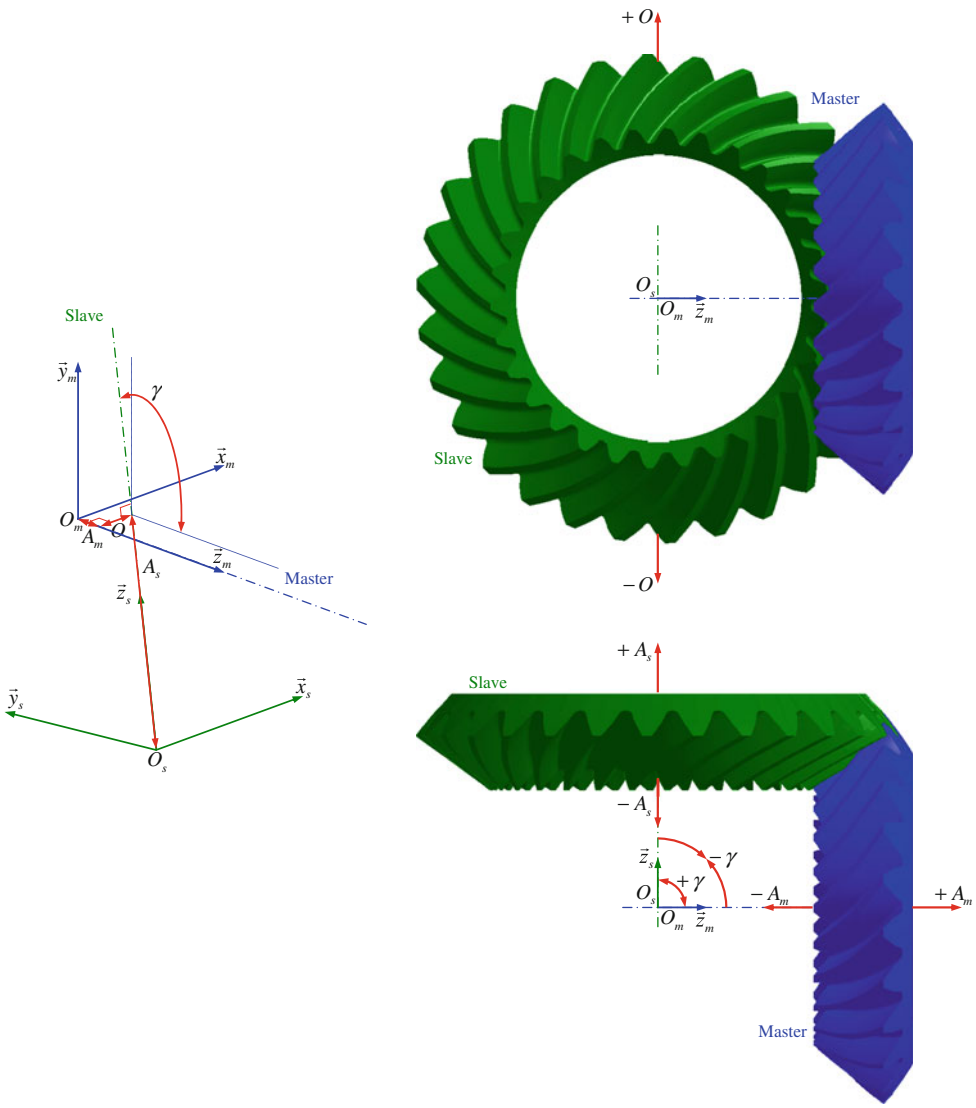

The existence condition of the tooth profile points on the given spheres is formalized by Eq. (11).

$$\sqrt{x_p^2(s_t,\phi_p)+y_p^2(s_t,\phi_p)+z_p^2(s_t,\phi_p)}-R_w=0 \qquad (11)$$

The tooth profile points are on the given cones if Eq. (12) is satisfied.

$$\arctan\left(\sqrt{y_p^2(s_t,\phi_p)+z_p^2(s_t,\phi_p)}/x_p(s_t,\phi_p)\right)-\gamma_w=0 \qquad (12)$$

The Eq. 10 is solved analytically and the two Eqs. (11) and (12) are solved numerically with the Newton–Raphson method. The Eqs. (10), (11) and (12) are solved simultaneously and the coordinates of the generated points are determined.

The tooth profile generation problem is more complex than the tooth root one. Two equations are numerically solved instead of one. The research process of the solutions is thus less stable. However, the presented mathematical formulation minimizes the number of equations which have to be solved using the Newton–Raphson algorithm. It makes simpler the debugging efforts during the development step to stabilize the iteration convergence. The simplicity and the robustness of the algorithm are easily improved.

2.2 Results

A computer application is coded with VBA in an EXCEL workbook. It generates a quite ruled and uniform mesh of the tooth flank surfaces. The generation process takes less than one second with the density shown on Fig. 10. The computer

used is a 2 CPU laptop with 1800 MHz clock rates. A VBA module is coded to draw splines and surfaces through the points. The CAO model shown in Fig. 10 is build with CATIA V5 software.

The simulated topographies are compared to the ones obtained with certified methods used in machine tool manufacturer software. The result is illustrated in Fig. 11. The distances between the two generated surfaces are lower than one micrometer. The minor gap can be due to slight numerical errors or rounding approximations in tabulating the modified roll coefficients.

3 Tooth contact analysis

3.1 Meshing simulation

The relative displacement of the two parts is taken into account in the meshing simulation algorithm. As shown in Fig. 12, it is made of four independent components: the axial displacement of the master part, the axial displacement of the slave part, the offset displacement also called hypoid displacement and the shaft angle. They can be set in the design process. However, they are generally due to mounting inaccuracies, under load distortions or bearing displacements. They are zero if the pitch apexes of the two parts are coincident. The sign of their value and the displacement direction are linked according to the Gleason rule. The axial displacement value is negative if the part moves toward the pitch apex. It is positive in the opposite direction. With the configuration represented in Fig. 12, the hypoid displacement value is negative if the gear moves down or else it is positive. The signs are opposite if the hand of spiral is changed. The shaft angle displacement value is negative if the two parts get closer or else it is positive.

The geometric and kinematic behavior of the contact pattern depends on the tooth flank topographies and their relative displacement. The tooth flank generation process previously explained is the core of the meshing simulation algorithm shown in Fig. 13. The contact points are selected among the whole points of the tooth profile. The stability of the algorithm only depends on the flank generation process. The research of the solution of the contact simulation problem is done on existing entities. This method does not imply non-convergence hazard due to a set of variable values out of the real field. It is based on the analysis of the angular distances between the tooth flanks in contact. A regular mesh is generated on the master tooth flank and its nodes are projected on the opposite slave tooth flank. The angular distances are computed between the master points and their respective projections on the slave surface. The master part can be either the pinion or the gear.

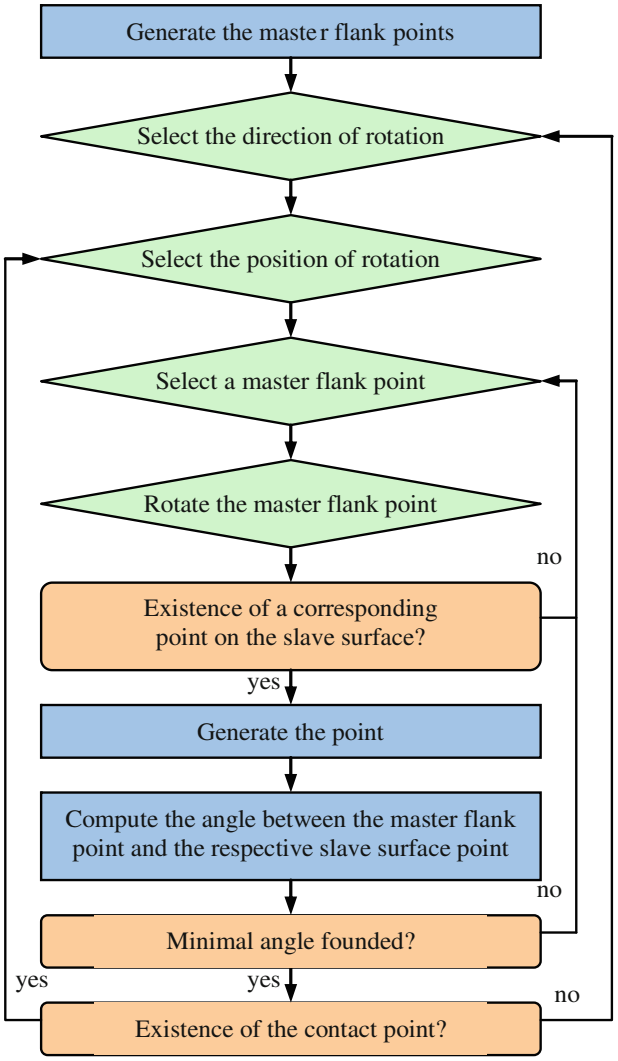

Fig. 13 Meshing simulation algorithm

For each position of the master part, all points of the master flank are successively considered. The position vector of the selected point in the master part system is known. It is written in the slave part system as shown in Fig. 14. The sphere radius and cone angle of the point in the slave part system are computed. The existence of the point inside the slave flank bounds is checked. If it is confirmed, the point of the slave surface is generated at the intersection of the sphere and cone using the tooth profile generation process previously explained.

The master flank rotates. The slave flank is fixed. For each meshing position of the master flank and for each node of the master flank mesh, the respective point existing on the slave flank is generated. Subsequently, the angle around the slave part axis between the two points is computed. The pair of points with the smallest angle is considered as the

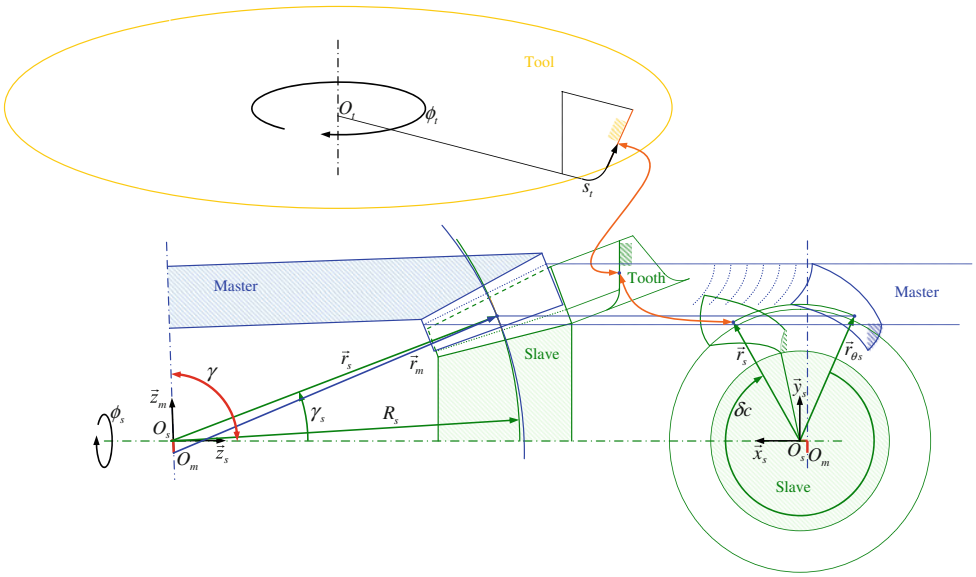

Fig. 14 Generation of the slave surface point

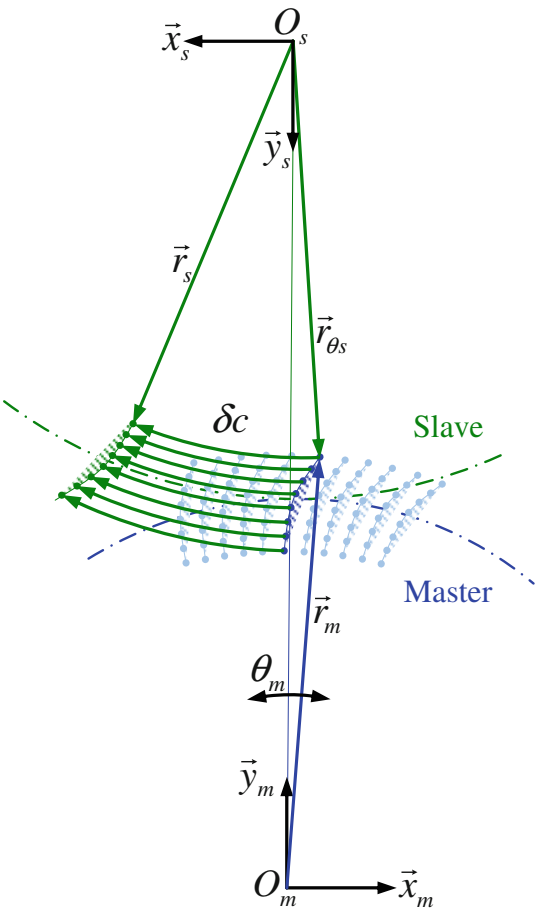

Fig. 15 Simulation of the contact

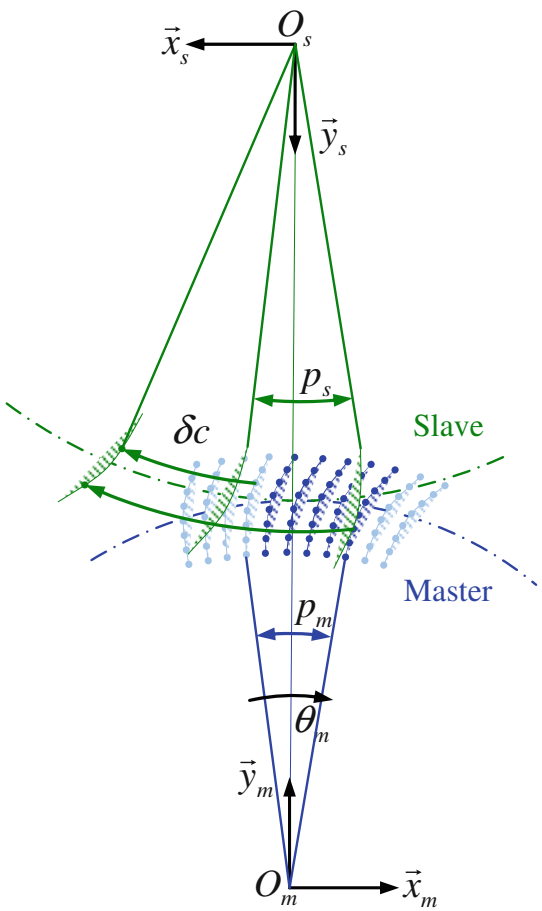

Fig. 16 Simulation of the meshing

approximated contact point. This approach is illustrated for a spur gear in Fig. 15.

The smallest angle value computed for each meshing position of the master part is compared with its value one pitch earlier. If the first is smaller than the second, the contact point exists in the meshing zone. Else, the contact point is out of the contact pattern and it does not exist. All the contact points of the contact pattern are selected in this way. This approach is illustrated for a spur gear in Fig. 16. The method can be quite easily coded in a computer program.

3.2 Results

The algorithm remains stable whatever the tooth flank topographies, whatever the relative position of the parts, whatever the discretizations of the master flank surface and the meshing motion. This quality is demonstrated with few examples. The basic data are given in Tables 1, 2, 3 and 4. The application runs on a 2 CPU laptop with 1800 MHz clock rates. Meshing simulations have been performed with low and high discretization densities. The computing process lasts 24 s in the first case and 246 s in the second. The unloaded contact pattern and transmission error are shown in Fig. 17. The contact points are selected among the master flank mesh nodes. That is why the contact pattern seems to be discontinuous. Actually, it should be a smooth curve. The transmission error is computed for each meshing position. A parabola fits the points. Its amplitude slightly changes with the model discretization but remains realistic. It gives an indication of the behavior of the mechanism. Indeed, noise is generated by the meshing motion and it increases with the amplitude of the transmission error.

The pinion and gear are mounted in a gear box. Their positioning is checked by comparing the locations of the real and virtual contact patterns. As shown in Fig. 17, the estimation of the simulated contact pattern location is good enough with a low accuracy. The high accuracy simulation is ten times longer than the low one. A high discretization density implies a long computing time and does not give more information.

The unloaded contact pattern is usually checked with a dedicated machine. The pinion and gear are positioned without relative displacement. A powder is spread on the active tooth flanks. The machine drives one of the two parts. The friction removes the powder in the meshing zone and the contact pattern appears. The simulation is validated by comparing the real and virtual contact patterns. They are shown in Fig. 18. Their locations are consistent. The real contact pattern is wider because the applied torque cannot be zero and the surfaces are not ideal. Furthermore, slight grinding and mounting tolerances are allowed for the checking test.

Table 1 Workpiece data

Workpiece	Pinion	Gear
Tooth flank	Concave	Convex
Number of teeth	23	30
Module (mm)	5	5
Whole depth (mm)	10.24	10.24
Addendum (mm)	5.6	3.65
Face angle (deg)	40.2	54.283
Pitch angle (deg)	37.483	52.517
Face width (mm)	29	29
Hand of spiral	Left hand	Right hand
Direction of rotation	Counter clockwise	Clockwise
Driving status	Driven	Driver

Table 2 Tool data

Mean diameter (mm)	143.013	152.392
Point width (mm)	1	1.910
Profile angle (deg)	19.225	20
Profile radius (mm)	392.872	∞
Point radius (mm)	0.76	1.2

Table 3 Machine settings

Cradle angle (deg)	60.891	300.183
Tilt angle (deg)	0	0
Swivel angle (deg)	0	0
Root angle (deg)	35.717	49.8
Radial distance (mm)	68.646	72.2
Work offset (mm)	−0.479	0
Sliding base (mm)	−0.937	−2.1
Machine center to cross point (mm)	−1.348	0
1st Modified roll coefficient	0.639404	0.794488
2nd Modified roll coefficient	−0.005814	0
3rd Modified roll coefficient	0.000598	0.001704
4th Modified roll coefficient	−0.000997	0
5th Modified roll coefficient	0.000023	−0.000024
6th Modified roll coefficient	−0.000168	0

Table 4 Axis displacements

Pinion axial displacement (mm)	0
Gear axial displacement (mm)	0
Hypoïd displacement (mm)	0
Shaft angle (deg)	90

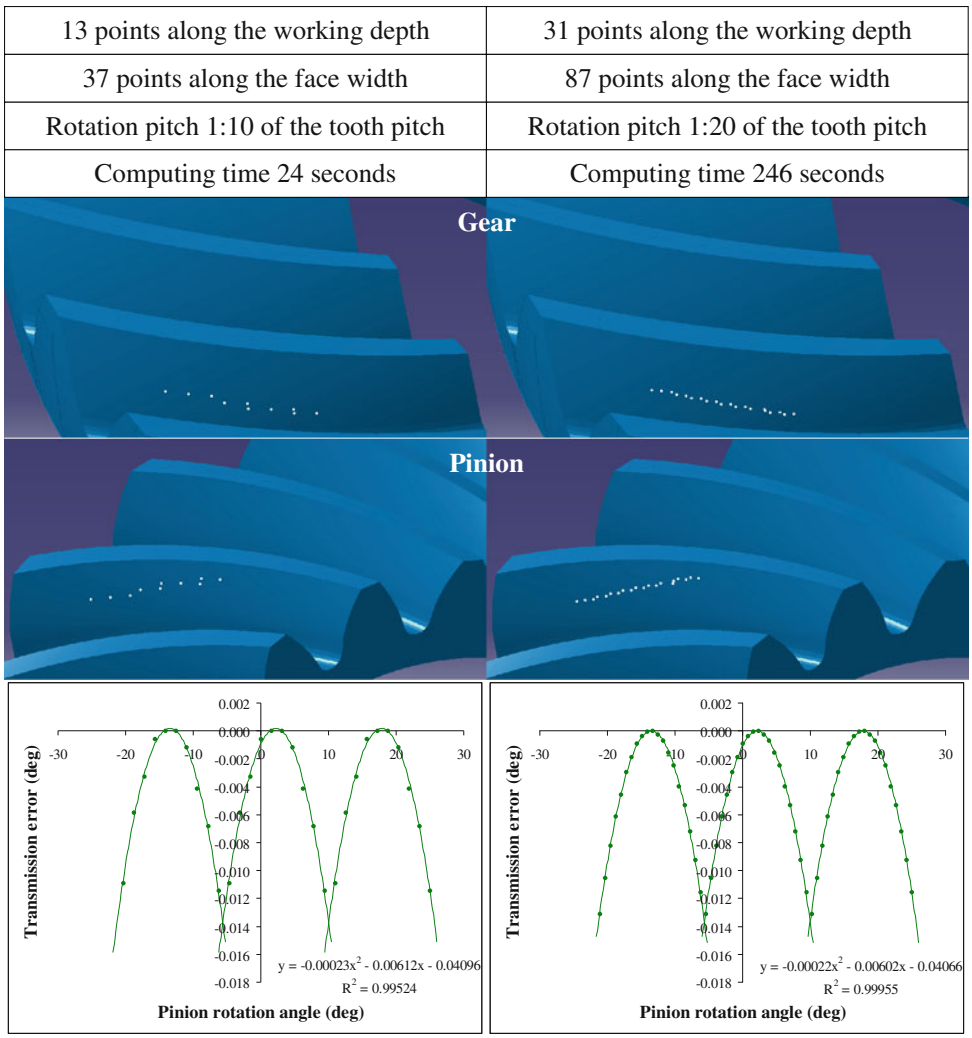

Fig. 17 Contact points and transmission error with low and high discretization density

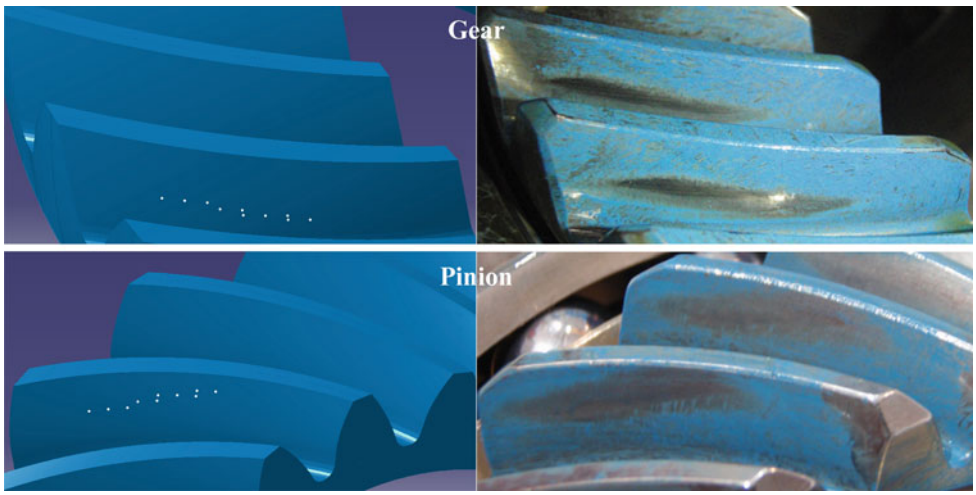

Fig. 18 Contact pattern checking test

4 Conclusion

In most tooth contact analysis approaches, the tooth flank modeling is the core of the meshing simulation algorithm. Each generated point is determined by numerically solving non-linear equations. The research of the solution can be managed with the Newton–Raphson method. This is a possible source of numerical instability. The proposed method

reduces significantly the number of equations to be simultaneously solved. It makes easier the algorithm development and the convergence management. The obtained unloaded meshing simulation gives a quite good and quick estimation of the contact pattern location. The stability of the algorithm only depends on the flank generation process. For each meshing position, the contact location is estimated among pairs of points. The existence of these points on their respective tooth flank is previously checked so the investigation field is mastered. It gives a robust and tolerant research process. The presented methods are coded in a computer application. The execution on a common laptop shows a sufficient computing efficiency enabling its implementation in iterative processes. The unloaded contact pattern location and the transmission error are commonly used to qualify the behavior of a gear. This paper lays down the bases of future works on the meshing motion control through an automated optimization process. Such an approach requires a really stable meshing simulation algorithm. The proposed methods insure a good speed, accuracy and stability.

References

1. Di Puccio, F., Gabiccini, M., Guiggiani, M.: Alternative formulation of the theory of gearing. Mech. Mach. Theory **40**, 613–637 (2005)
2. Di Puccio, F., Gabiccini, M., Guiggiani, M.: Generation and curvature analysis of conjugate surfaces via a new approach. Mech. Mach. Theory **41**, 382–404 (2006)
3. Di Puccio, F., Gabiccini, M., Guiggiani, M.: An invariant approach for gear generation with supplemental motions. Mech. Mach. Theory **42**, 275–295 (2007)
4. Dooner, D.B.: On the three laws of gearing. J. Mech. Des. **124**, 733–744 (2002)
5. Dooner, D.B., Seireg, A.A.: The Kinematic Geometry of Gearing. Wiley Interscience, New York (1995)
6. Fan, Q.: Computerized modeling and simulation of spiral bevel and hypoid gears manufactured by Gleason face hobbing process. J. Mech. Des. **128**, 1315–1327 (2006)
7. Fan, Q.: Enhanced algorithms of contact simulation for hypoid gear drives produced by face-milling and face-hobbing processes. J. Mech. Des. **129**, 31–37 (2007)
8. Fong, Z.H.: Mathematical model of universal hypoid generator with supplemental kinematic flank correction motions. J. Mech. Des. **122**, 136–142 (2000)
9. Gabiccini, M., Artoni, A., Di Puccio, F., Guiggiani, M.: A regularization method for hypoid gear synthesis using the invariant approach. In: 12th IFToMM World Congress, Besançon, France (2007)
10. Lin, G.C.Y., Tsay, C.B.P., Fong, Z.H.: Mathematical model of spiral bevel and hypoid gears manufactured by the modified roll method. Mech. Mach. Theory **32**, 121–136 (1997)
11. Litvin, F.L., Rahman, P., Goldrich, R. N.: Mathematical models for the synthesis and optimization of spiral bevel gear tooth surfaces. NASA CR-3553 (1982)
12. Litvin, F.L., Tsung, W.J., Coy, J.J., Handschuh, R.F.: New generation methods for spur, helical, and spiral bevel gears. NASA TM-88862 (1986)
13. Litvin, F.L., Chen, N.X.: Generation of gear tooth surfaces by application of CNC machines. NASA CR-195306 (1994)
14. Litvin, F.L., Fan, Q., Fuentes, A.: Computerized design, generation, and simulation of meshing and contact of face-milled formate cut spiral bevel gears. NASA CR-2001-210894 (2001)
15. Litvin, F.L., Fuentes, A., Fan, Q., Handschuh, R.F.: Computerized design, simulation of meshing, and contact and stress analysis of face-milled formate generated spiral bevel gears. Mech. Mach. Theory **37**, 441–459 (2002)
16. Litvin, F.L., Fuentes, A., Mullins, B.R., Woods, R.: Computerized design, generation, simulation of meshing and contact, and stress analysis of formate cut spiral bevel gear drives. NASA CR-2003-212336 (2003)
17. Litvin, F.L., Fuentes, A.: Gear Geometry and Applied Theory, 2nd edn. Cambridge University Press, Cambridge (2004)
18. Sheveleva, G.I., Volkov, A.E., Medvedev, V.I.: Algorithms for analysis of meshing and contact of spiral bevel gears. Mech. Mach. Theory **42**, 198–215 (2007)
19. Shih, Y.P., Fong, Z.H., Lin, G.C.Y.: Mathematical model for a universal face hobbing hypoid gear generator. J. Mech. Des. **129**, 38–47 (2007)
20. Vimercati, M.: Mathematical model for tooth surfaces representation of face-hobbed hypoid gears and its application to contact analysis and stress calculation. Mech. Mach. Theory **42**, 668–690 (2007)
21. Vogel, O., Griewank, A., Bär, G.: Direct gear tooth contact analysis for hypoid bevel gears. Comput. Methods Appl. Mech. Eng. **191**, 3965–3982 (2002)